Journal of Manufacturing Processes 15 (2013) 69–76

Contents lists available at SciVerse ScienceDirect

Journal of Manufacturing Processes

journal homepage: www.elsevier.com/locate/manpro

Technical paper

Analytical process damping stability prediction

Christopher T. Tyler, Tony L. Schmitz*

Mechanical Engineering and Engineering Science, University of North Carolina at Charlotte, Charlotte, NC, United States

ARTICLE INFO

Article history:
Received 8 June 2012
Received in revised form 2 November 2012
Accepted 26 November 2012
Available online 3 January 2013

Keywords:
Machining
Dynamics
Modeling
Tool wear
Process damping

ABSTRACT

This paper describes an analytical solution for turning and milling stability that includes process damping effects. Comparisons between the new analytical solution, time-domain simulation, and experiment are provided. The velocity-dependent process damping model applied in the analysis relies on a single coefficient similar to the specific cutting force approach to modeling cutting force. The process damping coefficient is identified experimentally using a flexure-based machining setup for a selected tool-workpiece pair (carbide insert-AISI 1018 steel). The effects of tool wear and cutting edge relief angle are also evaluated. It is shown that a smaller relief angle or higher wear results in increased process damping and improved stability at low spindle speeds.

1. Introduction

The analytical stability lobe diagram offers an effective predictive capability for selecting stable chip width-spindle speed combinations in machining operations [1–4]. However, the increase in allowable chip width provided at spindle speeds near integer fractions of the system's dominant natural frequency is diminished substantially at low spindle speeds where the stability lobes are closely spaced. Fortunately, the process damping effect can serve to increase the chatter-free chip widths at these low speeds. This increased stability at low spindle speeds is particularly important for hard-to-machine materials that cannot take advantage of the higher speed stability zones due to prohibitive tool wear at high cutting speeds.

Many researchers have investigated process damping in turning and milling operations. Early studies were carried out by Wallace and Andrew [5], Sisson and Kegg [6], Peters et al. [7], and Tlusty [8]. More recent efforts include:

- a plowing force model based on the interference between the tool and workpiece [9]
- the application of this plowing force model to milling operations [10–13]
- a mechanistic description of the contributions of shearing and plowing forces to process damping [14]
- a first-order Fourier transform representation of the interference between the tool and workpiece [15,16]
- numerical simulation of the nonlinear process damping stability model [17,18]
- an experimental investigation of the nonlinear process damping stability model [19]
- experimental identification of the process damping model [20,21].

These studies described process damping as energy dissipation due to interference between the cutting tool clearance face and machined surface during relative vibrations between the tool and workpiece. It was shown that, given fixed system dynamics, the influence of process damping increases at low spindle speeds because the number of undulations on the machined surface between revolutions/teeth increases, which also increases the slope of the wavy surface. This, in turn, leads to increased interference and additional energy dissipation.

In this paper, an iterative, analytical stability analysis is described that incorporates the effects of process damping. The analytical stability limit is validated using time-domain simulation and experiments. The paper is organized as follows. In the first section, process damping is described and the process damping force model is defined. Next, the stability algorithm is detailed. Results are then provided followed by the conclusions.

2. Process damping description

In descriptions of regenerative chatter in machining, the variable component of the instantaneous cutting force may be written as:

$$F = K_s b(Y_0 - Y), \tag{1}$$

* Corresponding author. Tel.: +1 7046878421.
E-mail address: tony.schmitz@uncc.edu (T.L. Schmitz).

1526-6125/$ – see front matter © 2012 The Society of Manufacturing Engineers. Published by Elsevier Ltd. All rights reserved.
http://dx.doi.org/10.1016/j.jmapro.2012.11.006

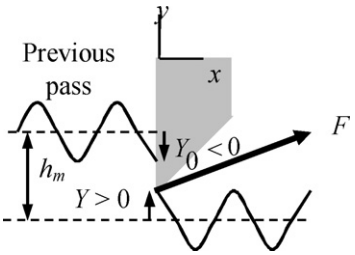

Fig. 1. The variable component of the cutting force, F, depends on the instantaneous chip thickness. The chip width is measured into the page; the mean chip thickness, h_m, is also identified.

where K_s is the specific cutting force (which depends on the tool-workpiece combination and, to a lesser extent, the cutting parameters), b is the chip width, Y_0 is the vibration amplitude in the surface normal direction, y, from the previous cutting pass, and Y is the current vibration amplitude. See Fig. 1. The underlying assumption in Eq. (1) is that there is no phase shift between the variable force and chip thickness; this is indicated by the real values of K_s and b. However, for low cutting speeds, V, it has been shown that a phase shift can occur. This behavior is captured by the phenomenon referred to as process damping. Practically speaking, the effect of process damping is to enable significantly higher chip widths at low cutting speeds than linear stability analyses predict.

To describe the physical mechanism for process damping, consider a tool moving on a sine wave while shearing away the chip [22]; see Fig. 2. Four locations are identified: (1) the clearance angle, γ, between the flank face of the tool and the work surface tangent is equal to the nominal relief angle for the tool; (2) γ is significantly decreased and can become negative (which leads to interference between the tool's relief face and surface); (3) γ is again equal to the nominal relief angle; and (4) γ is significantly larger than the nominal value.

At points 1 and 3 in Fig. 2, the clearance angle is equal to the nominal value so there is no effect due to cutting on the sinusoidal path. However, at point 2 the clearance angle is small (or negative) and the thrust force in the surface normal direction is increased. At point 4, on the other hand, the clearance angle is larger than the nominal and the thrust force is decreased. Because the change in force caused by the sinusoidal path is 90° out of phase with the displacement and has the opposite sign from velocity it is considered to be a viscous damping force (i.e., a force that is proportional to velocity). Given the preceding description, the process damping force, F_d, in the y direction can be expressed as a function of velocity, chip width, cutting speed, and a constant C [21]. See Eq. (2).

$$F_d = -C\frac{b}{V}\dot{y} \tag{2}$$

As a final note regarding the sinusoidal path description in Fig. 2, the damping effect is larger for shorter vibration wavelengths, λ, because the slope of the sinusoidal surface increases and, subsequently, the variation in clearance angle increases. The wavelength equation, provided in Eq. (3), shows that lower cutting speeds or

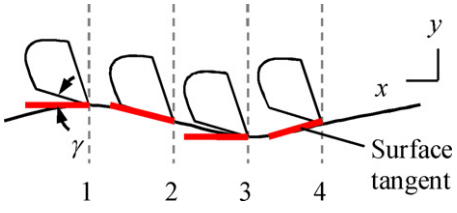

Fig. 2. Physical description of process damping. The clearance angle varies with the instantaneous surface tangent as the tool removes material on the sinusoidal surface.

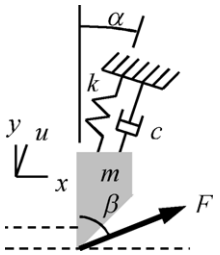

Fig. 3. Single degree of freedom turning model.

higher vibrating frequencies, f, gives shorter wavelengths and, subsequently, increased process damping.

$$\lambda = \frac{V}{f} \tag{3}$$

3. stability algorithm

3.1. Single degree of freedom turning

To describe the stability algorithm, consider the single degree of freedom turning model displayed in Fig. 3. Tlusty [22] defines the limiting stable chip width, $b_{\lim}$, for regenerative chatter using:

$$b_{\lim} = \frac{-1}{2K_s Re(G_{or})}, \tag{4}$$

where G_{or} is the oriented frequency response function, $G_{or} = \cos(\beta-\alpha)\cos(\alpha)G_u$. In this expression, β is the force angle relative to the surface normal, α is the angle between the u direction and the surface normal, and G_u is the frequency response function in the u direction. To relate the frequency-dependent $b_{\lim}$ vector to spindle speed, Ω, Eq. (5) is applied to define the relationship between Ω and the valid chatter frequencies, f_c (i.e., those frequencies where the real part of G_{or} is negative):

$$\frac{f_c}{\Omega} = N + \frac{\varepsilon}{2\pi}, \tag{5}$$

where $N = 0, 1, 2, \ldots$ is the integer number of waves per revolution (i.e., the lobe number) and $\varepsilon = 2\pi - 2\tan^{-1}(\mathrm{Re}(G_{or})/\mathrm{Im}(G_{or}))$ (rad) is the phase between the current vibration and the previous pass.

To incorporate the process damping force (which acts in the y direction), it is first projected into the u direction:

$$F_u = F_d\cos(\alpha) = -C\frac{b}{V}\dot{y}\cos(\alpha) = -\left(C\frac{b}{V}\cos(\alpha)\right)\dot{y}. \tag{6}$$

The final form of Eq. (6) emphasizes that the u projection of the process damping force is effectively a viscous damping term. Therefore, the force can be incorporated in the traditional regenerative chatter stability analysis by modifying the structural damping in G_u. As shown in Fig. 3, the single degree of freedom, lumped parameter dynamic model can be described using the mass, m, viscous damping coefficient, c, and spring stiffness, k. In the absence of process damping, the equation of motion in the u direction is:

$$m\ddot{u} + c\dot{u} + ku = F\cos(\beta-\alpha). \tag{7}$$

The corresponding frequency response function in the u direction is:

$$G_u = \frac{U}{F\cos(\beta-\alpha)} = \frac{1}{-m\omega^2 + ic\omega + k}, \tag{8}$$

where ω is the excitation frequency (rad/s). When process damping is included, however, the equation of motion becomes:

$$m\ddot{u} + c\dot{u} + ku = F\cos(\beta-\alpha) - (C\frac{b}{V}\cos(\alpha))\dot{y}. \tag{9}$$

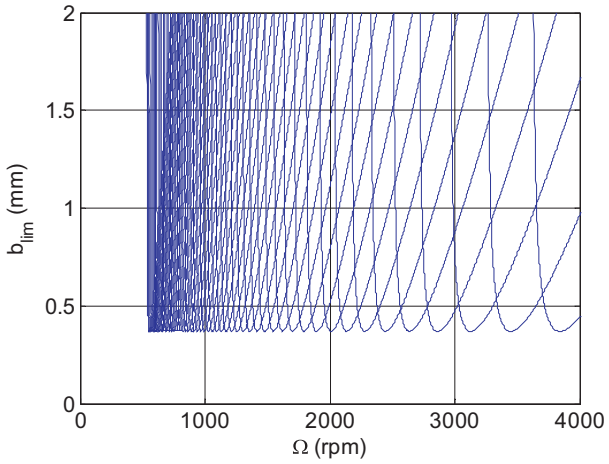

Fig. 4. Stability diagram for single degree of freedom model from Fig. 3 with $\alpha = 0$, $k = 6.48 \times 10^6$ N/m, $m = 0.561$ kg, $c = 145$ N s/m, $K_s = 2927 \times 10^6$ N/m^2, $\beta = 61.79^\circ$, $d = 0.035$ m, and $C = 0$.

Replacing $\dot{y}$ in Eq. (9) with $\cos(\alpha)\dot{u}$ gives:

$$m\ddot{u} + c\dot{u} + ku = F\cos(\beta - \alpha) - \left(C\frac{b}{V}\cos^2(\alpha)\right)\dot{u}. \tag{10}$$

Rewriting Eq. (10) to combine the velocity terms yields:

$$m\ddot{u} + \left(c + C\frac{b}{V}\cos^2(\alpha)\right)\dot{u} + ku = F\cos(\beta - \alpha), \tag{11}$$

where the new viscous damping coefficient is $c_{\text{new}} = c + C(b/V)\cos^2(\alpha)$. Replacing the original damping coefficient, c (from the structure dynamics only) with c_{new} enables process damping to be incorporated in the analytical stability model. The new frequency response function is:

$$G_u = \frac{U}{F\cos(\beta - \alpha)} = \frac{1}{-m\omega^2 + ic_{new}\omega + k}. \tag{12}$$

However, the new damping value is a function of both the spindle speed-dependent limiting chip width and the cutting speed. The cutting speed (m/s) depends on the spindle speed (rpm) and workpiece diameter (m) according to $V = (\pi d/60)\Omega$. Therefore, the b and Ω vectors must be known in order to implement the new damping value. This leads to the converging nature of the stability analysis that incorporates process damping. The following steps are completed for each lobe number, or N value (see Eq. (5)):

1. the analytical stability boundary is calculated with no process damping to identify initial b and Ω vectors
2. these vectors are used to determine the corresponding c_{new} vector
3. the stability analysis is repeated with the new damping value to determine updated b and Ω vectors
4. the process is repeated until the stability boundary converges.

To demonstrate the approach, consider the model in Fig. 3 with $\alpha = 0$, $k = 6.48 \times 10^6$ N/m, $m = 0.561$ kg, $c = 145$ N s/m, $K_s = 2927 \times 10^6$ N/m^2, $\beta = 61.79^\circ$, $d = 0.035$ m. The stability boundary with no process damping ($C = 0$) is shown in Fig. 4 for $N = 0$–60. It is observed that the limiting chip width approaches the asymptotic stability limit of 0.37 mm for spindle speeds below 1000 rpm.

Results of the converging procedure with process damping for the $N = 20$ stability boundary are provided in Fig. 5. Converging behavior is observed for the 10 iterations as the lobes move up and slightly to the right. Although a convergence criterion, such as a threshold percent difference between subsequent minimum values, could be implemented, a practical selection of 20 iterations

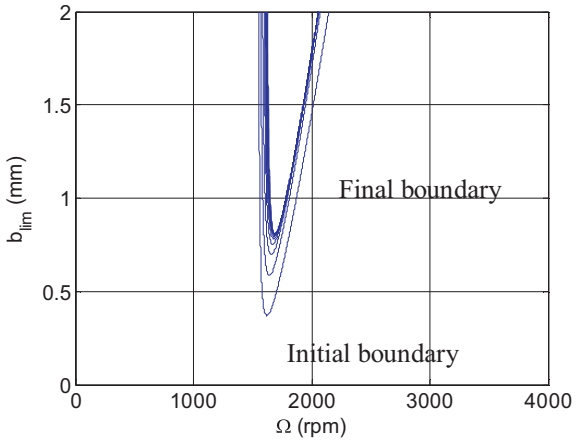

Fig. 5. Convergence demonstration ($N = 20$, 10 iterations) for single degree of freedom model from Fig. 3 with $\alpha = 0$, $k = 6.48 \times 10^6$ N/m, $m = 0.561$ kg, $c = 145$ N s/m, $K_s = 2927 \times 10^6$ N/m^2, $\beta = 61.79^\circ$, $d = 0.035$ m, and $C = 6.11 \times 10^5$ N/m.

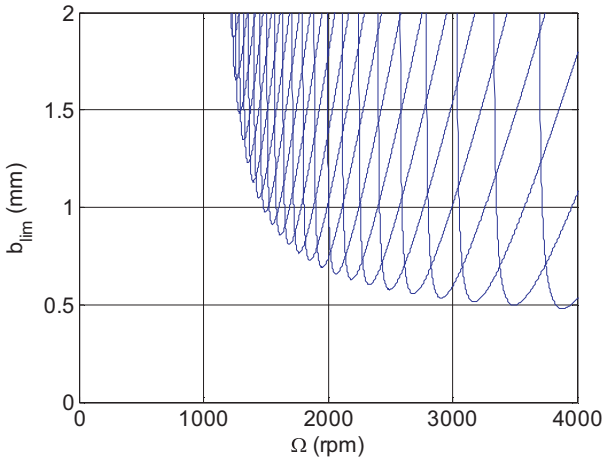

Fig. 6. Stability diagram for single degree of freedom model from Fig. 3 with $\alpha = 0$, $k = 6.48 \times 10^6$ N/m, $m = 0.561$ kg, $c = 145$ N s/m, $K_s = 2927 \times 10^6$ N/m^2, $\beta = 61.79^\circ$, $d = 0.035$ m, and $C = 6.11 \times 10^5$ N/m.

was applied for the diagrams in this study to ensure convergence. Fig. 6 displays the new stability diagram for $N = 0$–60 with $C = 6.11 \times 10^5$ N/m.

3.2. Two degree of freedom turning

The process damping model can be extended to consider vibration modes in two orthogonal directions as shown in Fig. 7. The analysis procedure is similar, but there are now two new damping values to be calculated: $c_{\text{new},1} = c_1 + C(b/V)\cos^2(\alpha_1)$ for the u_1 direction and $c_{\text{new},2} = c_2 + C(b/V)\cos^2(\alpha_2)$ for the u_2 direction. These

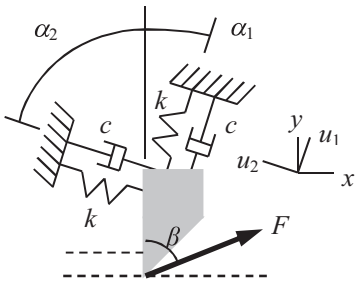

Fig. 7. Two degree of freedom turning model.

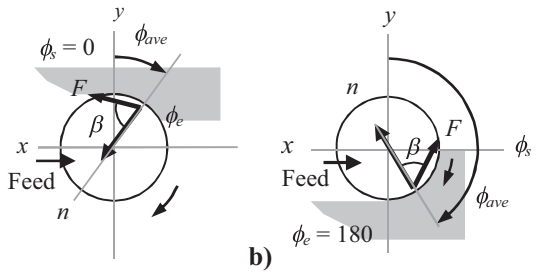

Fig. 8. (a) Geometry for up milling using the average tooth angle stability analysis (a 25% radial immersion cut is shown for illustrative purposes) and (b) model for down milling (a 50% radial immersion cut is shown). The vector n defines the average surface normal direction.

two damping values are used to update the G_{u_1} and G_{u_2} frequency response functions; see Eq. (12). The oriented frequency response function for this case is $G_{or} = \cos(\beta - \alpha_1)\cos(\alpha_1)G_{u_1} + \cos(\beta + \alpha_2)\cos(\alpha_2)G_{u_2}$.

3.3. Milling

Tlusty modified the previously described turning analysis to accommodate the milling process [3]. A primary obstacle to defining an analytical solution for milling stability (aside from the inherent time delay) is the time dependence of the cutting force direction. Tlusty solved this problem by assuming an average angle of the tooth in the cut, ϕ_{ave}, and, therefore, an average force direction. This produced an autonomous, or time invariant, system. He then made use of directional orientation factors, μ_x and μ_y, to first project this force into the x and y mode directions and, second, project these results onto the surface normal (in the direction of ϕ_{ave}). The new b_{lim} and Ω expressions for milling are provided in Eqs. (13) and (14), where N_t is the number of teeth on the cutter and N_t^* is the average number of teeth in the cut; see Eq. (15), where ϕ_s and ϕ_e (°) are the start and exit angles defined by the radial depth of cut. The ε equation remains the same as before.

$$b_{\text{lim}} = \frac{-1}{2K_s Re[G_{or}]N_t{}^*} \tag{13}$$

$$\frac{f_c}{\Omega N_t} = N + \frac{\varepsilon}{2\pi} \tag{14}$$

$$N_t{}^* = \frac{\varphi_e - \varphi_s}{360/N_t} \tag{15}$$

3.3.1. Up milling

The process damping force model defined in Eq. (2) was again applied, but the surface normal direction now depends on ϕ_{ave}. The geometry is shown in Fig. 8a, where n is the surface normal direction. The projection of the process damping force from the n direction onto the x direction is:

$$F_x = F_d \cos(90 - \phi_{\text{ave}}) = -\left(C\frac{b}{V}\cos(90 - \phi_{\text{ave}})\right)\dot{n}. \tag{16}$$

Note that the velocity term is now $\dot{n}$. Substituting $\dot{n} = \cos(90 - \phi_{\text{ave}})\dot{x}$ in Eq. (16) gives:

$$F_x = -\left(C\frac{b}{V}\cos^2(90 - \phi_{\text{ave}})\right)\dot{x}. \tag{17}$$

The new damping in the converging stability calculation for the x direction frequency response function, G_x, is therefore:

$$c_{\text{new},x} = c_x + C\frac{b}{V}\cos^2(90 - \phi_{\text{ave}}). \tag{18}$$

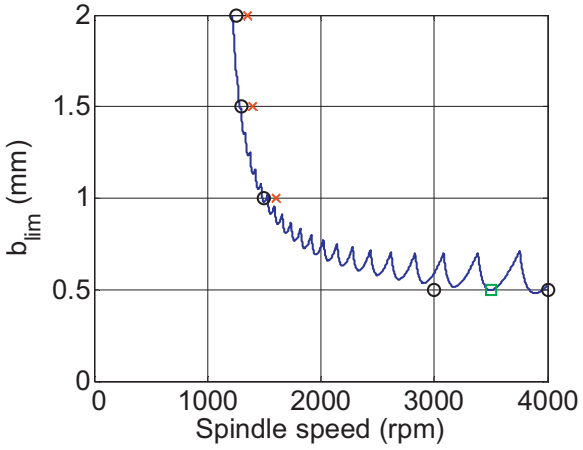

Fig. 9. Single degree of freedom turning model with $\alpha = 0$. The time domain simulation results are identified as: (circle) stable; (cross) unstable; and (square) marginally stable.

The new y direction damping is:

$$c_{\text{new},y} = c_y + C\frac{b}{V}\cos^2(180 - \phi_{\text{ave}}). \tag{19}$$

The oriented frequency response function for this case is $G_{or} = \mu_x G_x + \mu_y G_y$, where $\mu_x = \cos(\beta - (90 - \phi_{\text{ave}}))\cos(90 - \phi_{\text{ave}})$ and $\mu_y = \cos(180 - \phi_{\text{ave}} - \beta)\cos(180 - \phi_{\text{ave}})$.

3.3.2. Down milling

The geometry for the down milling case is shown in Fig. 8b. Using the same approach as described in the up milling case, the x and y direction damping values are provided in Eqs. (20) and (21).

$$c_{\text{new},x} = c_x + C\frac{b}{V}\cos^2(\phi_{\text{ave}} - 90) \tag{20}$$

$$c_{\text{new},y} = c_y + C\frac{b}{V}\cos^2(180 - \phi_{\text{ave}}) \tag{21}$$

The oriented frequency response function for this case is $G_{or} = \mu_x G_x + \mu_y G_y$, where $\mu_x = \cos(\beta + \phi_{\text{ave}} - 90)\cos(\phi_{\text{ave}} - 90)$, and $\mu_y = \cos(\beta - (180 - \phi_{\text{ave}}))\cos(180 - \phi_{\text{ave}})$.

4. Comparison with simulation

Both analytical analyses and time-domain simulations were completed to determine the process damping effects on turning and milling stability. The time-domain milling simulations were based on the 'Regenerative Force, Dynamic Deflection Model' described by Smith and Tlusty [23] where the damping force was included directly in the numerical integration of the system equations of motion; the simulation details are provided in [24]. The results are compared in the following sections.

4.1. Single degree of freedom turning

The model shown in Fig. 3 was considered. A comparison between the analytical stability lobes and time-domain simulation results are provided in Fig. 9. In this case $\alpha = 0$, $k = 6.48 \times 10^6$ N/m, $m = 0.561$ kg, and $c = 145$ N s/m, $K_s = 2927 \times 10^6$ N/m^2, $\beta = 61.8°$, and $C = 6.11 \times 10^5$ N/m. The workpiece diameter was 35 mm. In all instances, the time-domain results agree with the analytical stability limit.

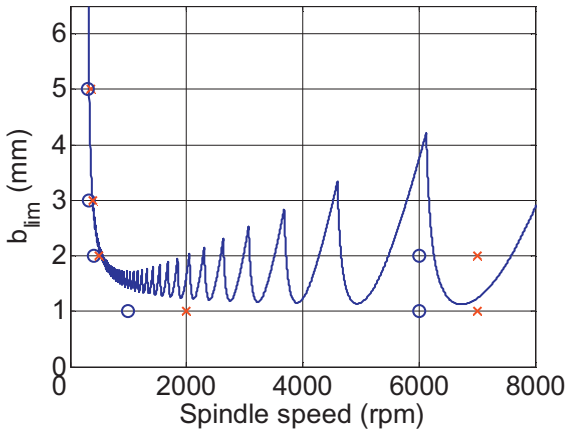

Fig. 10. Up milling results for 50% radial immersion. The time domain simulation results are identified as: (circle) stable and (cross) unstable.

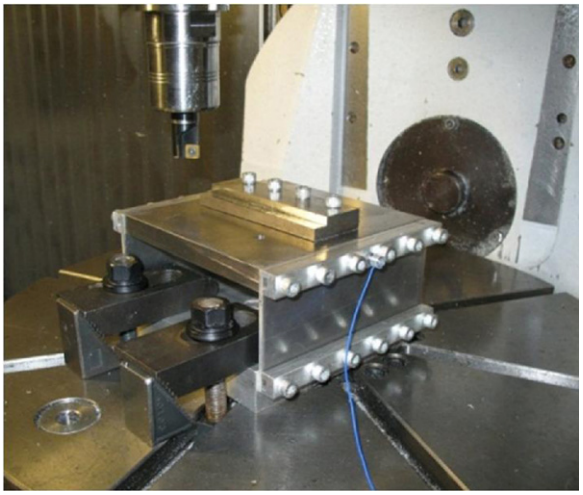

Fig. 11. Setup for milling stability tests. An accelerometer was used to measure the vibration signal during cutting.

4.2. Up milling

The model parameters for the three-tooth cutter were: $\phi_s = 0$ and $\phi_e = 90^\circ$ (50% radial immersion), the dynamics in both the x and y directions were described by $k = 9 \times 10^6$ N/m, $f_n = 900$ Hz, and $\zeta = 0.03$, and the force constants were $K_s = 2000 \times 10^6$ N/m, $\beta = 70^\circ$, and $C = 2 \times 10^4$ N/m. The comparison between the analytical stability lobes and time-domain simulation is provided in Fig. 10. The results match well.

5. Experimental identification of process damping coefficient

The process damping coefficient, C, for a selected tool-workpiece pair was identified through a series of cutting tests. A single-tooth indexable end mill was used to mill AISI 1018 steel workpieces secured to the top of single degree-of-freedom leaf-type flexure. The stability limit was identified over a grid of axial depths of cut and spindle speeds. Using the experimental stability boundary, the process damping coefficient was identified. The effects of insert relief angle and tool wear were examined. The flexure dynamics were also adjusted to determine the sensitivity of the process damping coefficient to changes in the system dynamics.

5.1. Setup description

In order provide convenient control of the system dynamics, a single degree-of-freedom, parallelogram leaf-type flexure was constructed to provide a flexible foundation for individual AISI 1018 steel workpieces; see Fig. 11. Because the flexure compliance was much higher than the tool-holder-spindle-machine, the stability analysis was completed using only the flexure's dynamic properties. A radial immersion of 50% and a feed per tooth of 0.05 mm/tooth was used for all conventional (up) milling tests.

In order to observe the sensitivity of the process damping coefficient to changes in the system dynamics, mass was added to the flexure in order to reduce the natural frequency; the added mass decreased the natural frequency by approximately 32%. The modal parameters for both cases are provided in Table 1. The x and y directions correspond to the flexible and stiff directions of the flexure, respectively, where y is the feed direction.

An accelerometer (PCB Piezotronics model 352B10) was used to measure the vibration during cutting. The frequency content of the accelerometer signal was used in combination with the machined surface finish to establish stable/unstable performance, i.e., cuts that exhibited significant frequency content at the flexure's x direction natural frequency, rather than the tooth passing frequency, were considered to be unstable.

In order to study the influence of relief angle under milling conditions, two single-tooth indexable square end mills of similar diameter were used: (1) 18.54 mm diameter with a 15° relief angle (Kennametal model KICR-0.73-SD3-033.3C); and (2) 19.05 mm diameter with an 11° relief angle (Cutting Tool Technologies model DRM-03). Both cutting tools had a 0° rake angle and the inserts had no edge preparation.

The cutting force coefficients were identified under stable cutting conditions using a cutting force dynamometer (Kistler model 9257B). For the 18.54 mm diameter cutter, the specific cutting force, K_s, and cutting force direction, β, were determined to be 2359.1 N/mm^2 and 63.5°, respectively. For the 19.05 mm diameter cutter, the values were 2531.0 N/mm^2 and 62.0°. A linear regression to the mean cutting force over a series of tests at various feed per tooth values was used to identify the cutting force model values [24].

5.2. Process damping coefficient identification

Conventional linear stability analysis (i.e., $C = 0$ N/m) was first used to validate the stability behavior at higher speeds for the flexure setup. As seen in Fig. 12, the predicted behavior was observed experimentally. Additionally, the critical limiting chip width, $b_{lim,cr}$, was identified to be approximately 1 mm for the 228 Hz setup; this result also agreed with the analytical prediction. A similar approach was used to validate the stability boundary for the 156 Hz setup. The critical stability limit was approximately 0.4 mm for this system; see Fig. 13.

A grid of test points at low spindle speed was next selected to investigate the process damping behavior. Based on the stable/unstable cutting test results, a single variable residual sum of squares (*RSS*) estimation was applied to identify the process damping coefficient that best represented the experimental stability

Table 1
Modal parameters for flexure with and without added mass.

	Direction	Viscous damping ratio	Modal stiffness (MN/m)	Natural frequency (Hz)
No mass	x	0.063	2.77	228
	y	0.037	174	1482
Added mass	x	0.018	4.37	156
	y	0.028	276	1137

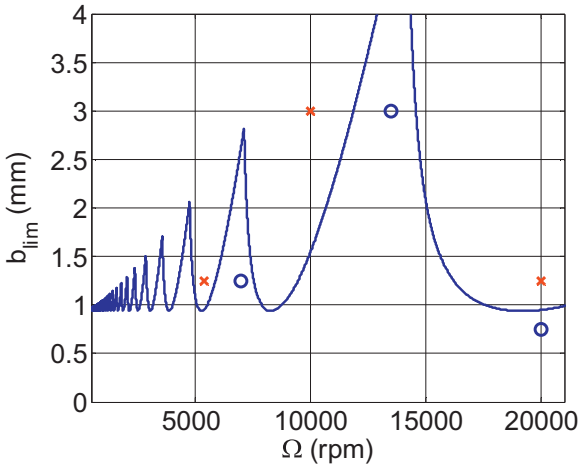

Fig. 12. Stability lobe validation for the 228 Hz setup.

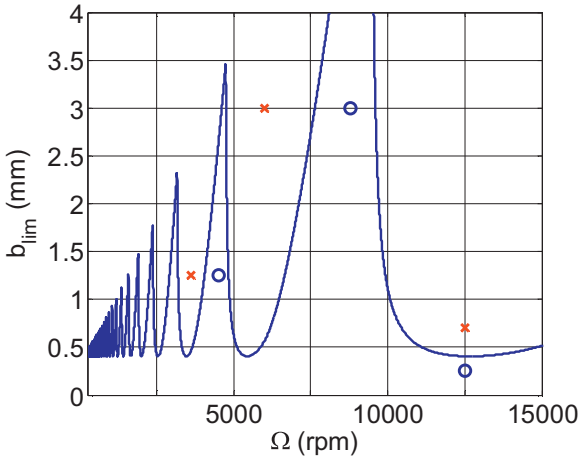

Fig. 13. Stability lobe validation for the 156 Hz setup.

boundary; see Fig. 14. The spindle-speed dependent experimental stability limit, b_i, was selected to be the midpoint between the stable and unstable points at the selected spindle speed. The sum of squares of residuals is given by Eq. (22), where is the analytical stability boundary and n is the number of test points. A range of process damping coefficients was selected and the *RSS* value was calculated for each corresponding stability limit. The C value that

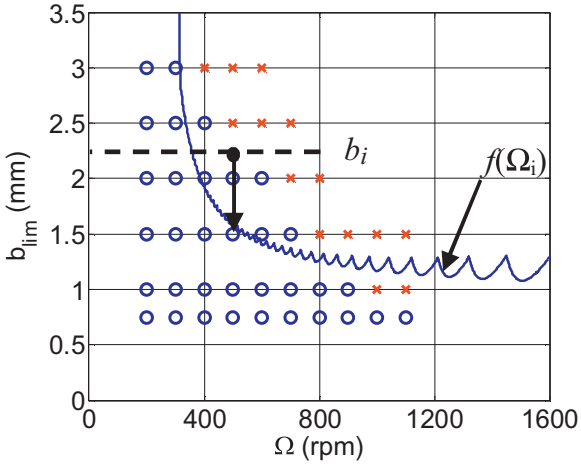

Fig. 14. Description of variables for *RSS* estimate of process damping coefficient.

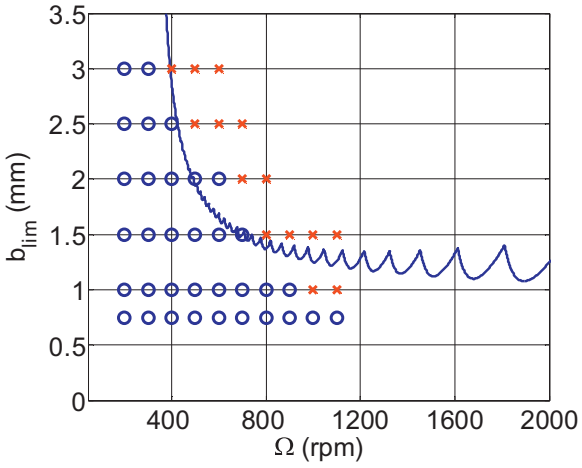

Fig. 15. Up milling stability boundary for 50% radial immersion, 15° relief angle, low wear milling tests using the 228 Hz flexure setup ($C = 2.5 \times 10^5$ N/m).

corresponded to the minimum *RSS* value was selected to identify the final stability boundary for all test conditions.

$$RSS = \sum_{i=1}^{n} (b_i - f(\Omega_i))^2 \tag{22}$$

Using the minimum *RSS* method, stability testing was performed for the 18.54 mm diameter, 15° relief angle end mill. Because flank wear can affect the process damping behavior, the flank wear width (FWW) was limited to less than 100 μm for these tests. A portable microscope (60× magnification) was used to record digital images of the flank surfaces at regular intervals. A process damping coefficient of $C = 2.5 \times 10^5$ N/m was found to best fit the data for the 228 Hz system (50% radial immersion up milling). The corresponding stability boundary is provided in Fig. 15. The procedure was repeated for the 156 Hz setup and a process damping coefficient of $C = 2.6 \times 10^5$ N/m was identified. These results are displayed in Fig. 16. It should be noted that in some cases stable cutting conditions lie within the predicted unstable region. This is likely due to the simplicity of the process damping force model. Later in this paper a confidence region for the stability boundary is established.

Tests were then performed using the 19.05 mm diameter, 11° relief angle end mill. The same procedure was following and the FWW was again limited to be less than 100 μm for all cuts. The

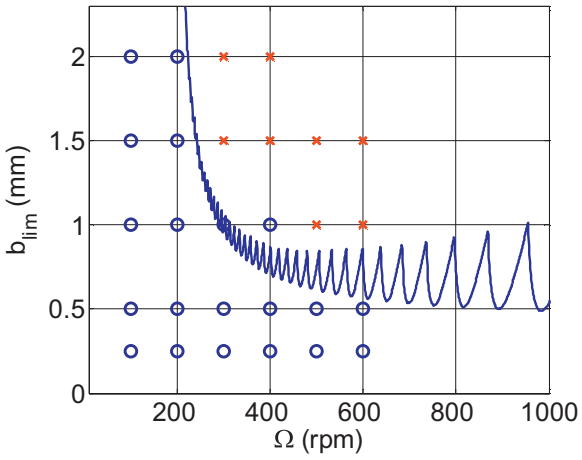

Fig. 16. Up milling stability boundary for 50% radial immersion, 15° relief angle, low wear milling tests using the 156 Hz flexure setup ($C = 2.6 \times 10^5$ N/m).

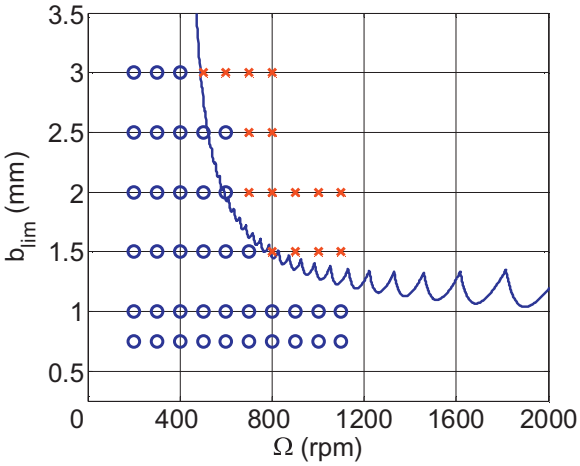

Fig. 17. Up milling stability boundary for 50% radial immersion, 11° relief angle, low wear milling tests using the 228 Hz flexure setup ($C = 3.3 \times 10^5$ N/m).

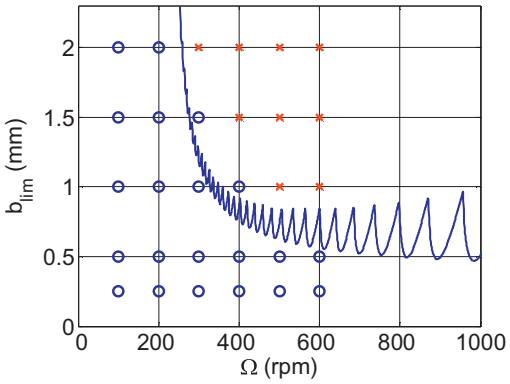

Fig. 18. Up milling stability boundary for 50% radial immersion, 11° relief angle, low wear milling tests using the 156 Hz flexure setup ($C = 3.3 \times 10^5$ N/m).

process damping coefficient for both the 228 Hz and 156 Hz setups was 3.3×10^5 N/m. See Figs. 17 and 18.

The low wear stability test results are summarized in Table 2. The process damping coefficient for the 228 Hz setup increased by 32% for the 11° relief angle tool relative to the 15° relief angle tool. A 27% increase was observed for the 156 Hz setup.

5.3. Tool wear effects on process damping coefficient

In order to explore the effect of tool wear on the process damping performance, tests were completed using worn tools where the FWW was maintained at a level of 200 μm. For the 15° relief angle tool, the specific cutting force and cutting force direction were 2441.0 N/mm^2 and 63.5°, respectively; this represents a 3.5% increase in the specific cutting force relative to the unworn tool tests. However, the process damping coefficient was found to increase from the unworn tool tests by 20% for the 228 Hz setup and 31% for the 156 Hz setup. Similarly, for the 11° cutter, the cutting force parameters experienced only a slight change ($K_s = 2550.2$ N/mm^2 and $\beta = 62.0°$). However, the process damping coefficient increased by 15.2% for both flexure setups (see Table 3).

Table 2
Comparison of process damping coefficients for low wear tests.

Relief angle (°)	C (N/m) for the 228 Hz setup	C (N/m) for the 156 Hz setup
15	2.5×10^5	2.6×10^5
11	3.3×10^5	3.3×10^5

Table 3
Comparison of process damping coefficients for moderate wear tests.

Relief angle (°)	C (N/m) for the 228 Hz setup	C (N/m) for the 156 Hz setup
15	3.0×10^5	3.4×10^5
11	4.0×10^5	3.8×10^5

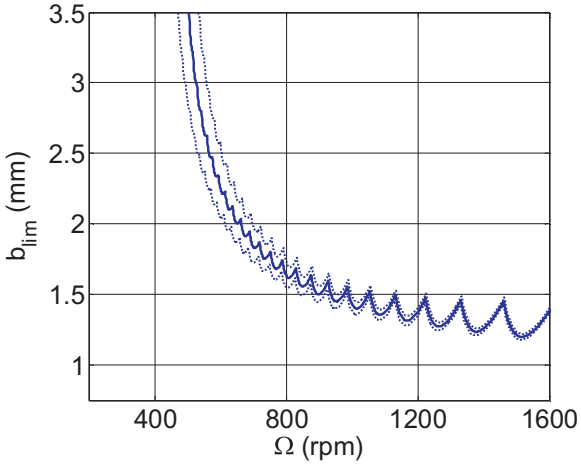

Fig. 19. Up milling stability confidence region for 50% radial immersion, 11° relief angle milling tests using the 228 Hz flexure setup with an unworn cutting edge ($C = (3.2 \pm 0.15) \times 10^5$ N/m).

5.4. Repeatability

Repeat testing was performed using the 19.05 mm diameter, 11° relief angle cutting tool in order to observe the variability in the process damping coefficient. A series of three additional cutting tests were performed on the 228 Hz system with an unworn insert. The three process damping coefficients were: 3.3×10^5 N/m, 3.3×10^5 N/m, and 2.9×10^5 N/m. Assuming a normal distribution, a two-sided 90% confidence level was computed for this small sample size. The confidence interval for the population mean was: $C = (3.2 \pm 0.15) \times 10^5$ N/m. Fig. 19 illustrates the corresponding confidence region.

6. Conclusions

An analytical solution for machining stability while considering process damping was provided, where the process damping model relied on a single coefficient, C. This is analogous to the specific cutting force, K_s, approach to modeling cutting force. Stability testing was completed using a single degree of freedom flexure to identify the process damping coefficient for low-speed milling of AISI 1018 steel under various conditions. It was demonstrated that a reduction in the relief angle and an increase in flank wear of the cutting edge increased the process damping coefficient.

Process damping is particularly important for hard-to-machine materials, such as titanium, nickel super alloys, and hardened steels. In these instances, tool wear generally prohibits higher surface speeds and the use of the large stable zones available at high spindle speeds. This limits the spindle speed to low values, which decreases the material removal rate. However, by exploiting process damping, higher stable axial depths and material removal rates can be achieved.

References

[1] Tlusty J, Polacek M. The stability of machine tools against self-excited vibrations in machining. In: Proceedings of the ASME international research in production engineering conference. 1963. p. 465–74.

[2] Tobias SA. Machine tool vibrations. Glasgow: Blackie and Sons, Ltd.; 1965.
[3] Tlusty J, Zaton W, Ismail F. Stability lobes in milling. Annals of the CIRP 1983;32(1):309–13.
[4] Altintas Y, Budak E. Analytical prediction of stability lobes in milling. Annals of the CIRP 1995;44(1):357–62.
[5] Wallace PW, Andrew C. Machining forces: some effects of tool vibration. Journal of Mechanical Engineering Science 1965;7:152–62.
[6] Sisson TR, Kegg RL. An explanation of low-speed chatter effects. Journal of Engineering for Industry 1969;91:951–8.
[7] Peters J, Vanherck P, Van Brussel H. The measurement of the dynamic cutting coefficient. Annals of the CIRP 1971;21(2):129–36.
[8] Tlusty J. Analysis of the state of research in cutting dynamics. Annals of the CIRP 1978;27(2):583–9.
[9] Wu DW. A new approach of formulating the transfer function for dynamic cutting processes. Journal of Engineering for Industry 1989;111:37–47.
[10] Elbestawi MA, Ismail F, Du R, Ullagaddi BC. Modelling machining dynamics damping in the tool-workpiece interface. Journal of Engineering for Industry 1994;116:435–9.
[11] Lee BY, Trang YS, Ma SC. Modeling of the process damping force in chatter vibration. International Journal of Machine Tools and Manufacture 1995;35:951–62.
[12] Abraria F, Elbestawi MA, Spencea AD. On the dynamics of ball end milling: modeling of cutting forces and stability analysis. International Journal of Machine Tools and Manufacture 1998;38:215–37.
[13] Ahmadi K, Ismail F. Machining chatter in flank milling. International Journal of Machine Tools and Manufacture 2010;50:75–85.
[14] Huang CY, Wang JJ. Mechanistic modeling of process damping in peripheral milling. Journal of Manufacturing Science and Engineering 2007;129:12–20.
[15] Chiou YS, Chung ES, Liang SY. Analysis of tool wear effect on chatter stability in turning. International Journal of Mechanical Sciences 1995;37:391–404.
[16] Chiou RY, Liang SY. Chatter stability of a slender cutting tool in turning with tool wear effect. International Journal of Machine Tools and Manufacture 1998;38:315–27.
[17] Chandiramani NK, Pothala T. Dynamics of 2-dof regenerative chatter during turning. Journal of Sound and Vibration 2006;290:448–64.
[18] Jemielniak K, Widota A. Numerical simulation of non-linear chatter vibration in turning. International Journal of Machine Tools and Manufacturing 1989;29:239–47.
[19] Ahmadi K, Ismail F. Experimental investigation of process damping nonlinearity in machining chatter. International Journal of Machine Tools and Manufacture 2010;50:1006–14.
[20] Budak E, Tunc LT. A new method for identification and modeling of process damping in machining. Journal of Manufacturing Science and Engineering 2009;131:051019/1–51019.
[21] Altintas Y, Eynian M, Onozuka H. Identification of dynamic cutting force coefficients and chatter stability with process damping. Annals of the CIRP 2008;57(1):371–4.
[22] Tlusty J. Manufacturing processes and equipment. Upper Saddle River, NJ: Prentice Hall; 2000.
[23] Smith S, Tlusty J. An overview of modeling and simulation of the milling process. Journal of Engineering for Industry 1991;113:169–75.
[24] Schmitz T, Smith S. Machining dynamics: frequency response to improved productivity. New York, NY: Springer; 2009.